Constrained RIS Phase Profile Optimization and Time Sharing for Near-field Localization

N.B. When citing this work, cite the original published paper.

(article starts on next page)

Constrained RIS Phase Profile Optimization and Time Sharing for Near-field Localization

Moustafa Rahal[*‡], Benoît Denis[*], Kamran Keykhosravi[†],
Musa Furkan Keskin[†], Bernard Uguen[‡], Henk Wymeersch[†]
[*] CEA-Leti, Université Grenoble Alpes, F-38000 Grenoble, France
[†] Department of Electrical Engineering, Chalmers University of Technology, Gothenburg, Sweden
[‡] Université Rennes 1, IETR - UMR 6164, F-35000 Rennes, France

Abstract—The rising concept of reconfigurable intelligent surface (RIS) has promising potential for Beyond 5G localization applications. We herein investigate different phase profile designs at a reflective RIS, which enable non-line-of-sight positioning in nearfield from downlink single antenna transmissions. We first derive the closed-form expressions of the corresponding Fisher information matrix (FIM) and position error bound (PEB). Accordingly, we then propose a new localization-optimal phase profile design, assuming prior knowledge of the user equipment location. Numerical simulations in a canonical scenario show that our proposal outperforms conventional RIS random and directional beam codebook designs in terms of PEB. We also illustrate the four beams allocated at the RIS (i.e., one directional beam, along with its derivatives with respect to space dimensions) and show how their relative weights according to the optimal solution can be practically implemented through time sharing (i.e., considering feasible beams sequentially).

Index Terms—Nearfield localization, non-line-of-sight, RIS phase optimization.

I. INTRODUCTION

Among the potential 6G technologies, reconfigurable intelligent surfaces (RISs) stand out for their ability to purposely shape wireless environments [1]. A typical RIS generally comprises a large number of controllable elements, which can be adjusted (typically, in terms of their phases) by means of lightweight electronics so as to behave as electromagnetic mirrors or lenses. RISs also have appealing applications to spatial awareness and sensing [2], for instance to overcome line-of-sight (LoS) blockages through newly induced multipath components, hence making localization feasible when conventional systems would fail. Beyond, they can be also beneficial to control and locally/timely improve localization accuracy when the LoS path is present. Such flexibility and synergies between data communication and on-demand localization services are expected to be among the main drivers in future 6G systems, thus making RIS a key enabling technology. Beyond quite extensive works on wireless localization exploiting the spherical wavefront of incoming signals at large receiving RISs (e.g., [3]–[6]), other recent research studies have also considered the use of passive reflective RISs in the context of parametric multipath-aided positioning, in both LoS (e.g., [7]–[11]) and non-line-of-sight (NLoS) (e.g., [12], [13]) conditions.

An important challenge with RIS lies in the optimization of their profiles (i.e., their reflection coefficients and/or their phases), before or after performing channel estimation. For
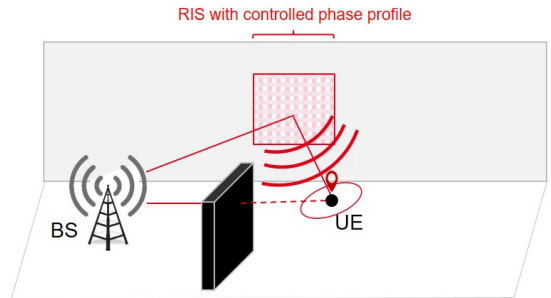

Fig. 1: Typical NLoS positioning scenario with one single reflective RIS in nearfield over single-input-single-output downlink transmissions.

data communication purposes, the latter problem can be solved based on the estimated cascaded channel responses or using a priori location information [14]. The former problem can be solved with a variety of approaches, including that maximizing recovery performance, based on the Discrete Fourier Transform (DFT) and Hadamard matrices, or harnessing external location information too [15]. As for RISs-based localization more specifically, in [7], joint RIS selection and directional reflection beam design has been considered while assuming prior knowledge of the user equipment (UE) location, which intuitively corresponds to concentrating the reflected power towards the UE and accordingly, increase signal-to-interference-and-noise-ratio (SINR) at the UE. Alternatively, the authors in [11], [12] have used simpler random RIS phase profiles for asynchronous positioning in a downlink single-input-single-output (SISO) multi-carrier (MC) transmission context. This scheme does not require any prior information (neither about the channel, nor about the UE location), but is not optimal under a priori UE location information. Finally, in [8], RIS phases and beamformers are jointly optimized with respect to both the position error bound (PEB) and the orientation error bound (OEB) in a generic multiple inputs multiple outputs (MIMO) MC context, based on a signal-to-noise ratio (SNR) criterion.

In this paper, in contrast to the previous contributions and leveraging the simpler SISO downlink positioning scheme of [11], [12], we design suitable phase profiles at a reflective RIS through PEB optimization in an NLoS context (See Fig. 1),while putting more emphasis on practical implementation constraints (typically, forcing the RIS complex element response to lie on the unit-circle). Beyond making
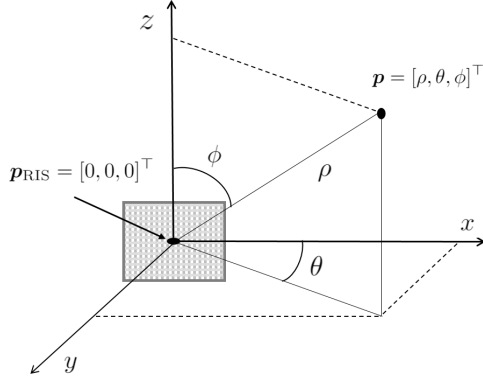
Fig. 2: Problem geometry for a UE in $\boldsymbol{p}$ and the RIS phase center in $\boldsymbol{p}_{\mathrm{RIS}}$, as the origin of both spherical and Cartesian coordinates systems.

localization feasible (with significantly degraded accuracy in comparison with LoS conditions though) [12], the goal is to further optimize NLoS positioning performance, while relying on direct localization using the RIS-reflected path (i.e., as estimated at the UE over downlink transmissions). Our main contributions are: *(i)* we derive closed-form expressions of both the FIM and the PEB, while assuming a generic nearfield-compliant formulation for the RIS response, *(ii)* we show how the PEB optimization problem can be solved efficiently and how localization-optimized RIS phase profiles are obtained, considering practical time sharing among different profiles; *(iii)* we compare the performance of the resulting localization-optimal phase profiles, along with its constrained (and thus sub-optimal) variants, with that of conventional random and directional designs, and *(iv)* we discuss the shapes taken by the RIS beam and its successive derivatives with respect to the 3D dimensions (in spherical coordinates) in light of our specific estimation problem.

Notations: Vectors and matrices are denoted, respectively, with a lower-case and upper-case bold letter (e.g., $\boldsymbol{x}, \boldsymbol{X}$), while subscripts are used to denote their indices. Transpose, conjugate and hermitian conjugate are respectively denoted by $(.)^{\top}$, $(.)^{*}$ and $(.)^{\mathsf{H}}$. Furthermore, the operator $\mathrm{tr}(\boldsymbol{X})$ denotes the trace of matrix $\boldsymbol{X}$ and $\mathrm{diag}(\boldsymbol{x})$ denotes a diagonal matrix with diagonal elements defined by vector $\boldsymbol{x}$. Finally, $\|\cdot\|$ is the l_2-norm operator and $(.)^{\star}$ denotes the solution of an optimization problem.

II. SYSTEM MODEL

We consider a 3D localization setup consisting of a single-antenna base station (BS), a single-antenna UE and a planar reflective RIS composed of M elements. The corresponding 3D locations are expressed in the same global reference coordinates system as follows: $\boldsymbol{p}_{\mathrm{BS}} \in \mathbb{R}^{3\times 1}$ is a vector containing the known BS coordinates, $\boldsymbol{p}_{\mathrm{RIS}} \in \mathbb{R}^{3\times 1}$ is a vector containing the known coordinates of the RIS center, $\boldsymbol{p}_m \in \mathbb{R}^{3\times 1}$ is a vector containing the known coordinates of the m-th element in the RIS, and $\boldsymbol{p} \in \mathbb{R}^{3\times 1}$ is a vector containing UE's unknown coordinates, expressed as $[x, y, z]^{\top}$ in the Cartesian coordinates system or $[\rho, \theta, \phi]^{\top}$ in the spherical coordinates system, where ρ is the range from the system's origin, θ is the

azimuth angle measured from the positive x-axis and likewise, ϕ is the elevation angle from the positive z-axis. Without loss of generality, in the sequel, we choose the RIS phase center as the origin of the coordinates system. The geometry of the problem is illustrated in Fig. 2. We consider a millimeter wave (mmWave) downlink communication scenario in presence of LoS blockage, where the BS broadcasts a narrowband pilot signal $x_t \in \mathbb{C}$ with a bandwidth W over T transmissions and transmit power P_{tx}. In NLoS, the complex signal $y_t \in \mathbb{C}$ received by the UE at time t after RIS reflection is

$$y_t = \beta \boldsymbol{a}^{\top}(\boldsymbol{p}) \boldsymbol{\Omega}_t \boldsymbol{a}(\boldsymbol{p}_{\mathrm{BS}}) x_t + n_t, \qquad (1)$$

where $\boldsymbol{a}(.) \in \mathbb{C}^{M\times 1}$ is a steering vector representing the RIS response, in its most generic formulation (i.e., encompassing the nearfield (NF) regime like in [12]), whose m-th entry with respect to the m-th RIS element $\boldsymbol{p}_m$ and the RIS phase center $\boldsymbol{p}_{\mathrm{RIS}}$ is

$$[\boldsymbol{a}(\boldsymbol{p})]_m = \exp\left(-\jmath \frac{2\pi}{\lambda}\left(\|\boldsymbol{p} - \boldsymbol{p}_m\| - \|\boldsymbol{p} - \boldsymbol{p}_{\mathrm{RIS}}\|\right)\right). \qquad (2)$$

Moreover, the transmit symbol energy is defined as $E_s = \mathbb{E}\{|x_t|^2\} = P_{\mathrm{tx}}/W$ with total transmit energy $E_{\mathrm{tot}} = E_s M T$, $n_t \sim \mathcal{CN}(0, N_0)$ is the independent and identically distributed (i.i.d.) observation noise of power spectral density N_0, β is the time-invariant complex channel gain for the reflected path and $\boldsymbol{\Omega}_t = \mathrm{diag}(\boldsymbol{\omega}_t)$ where $\boldsymbol{\omega}_t \in \mathbb{C}^{M\times 1}$ is the t-th phase profile vector applied across the M RIS elements. This received signal can hence be vectorized over T transmissions into $\boldsymbol{y} \in \mathbb{C}^{T\times 1}$ as follows[1]

$$\boldsymbol{y} = \sqrt{E_s}\beta \boldsymbol{F}^{\top}\boldsymbol{a}(\boldsymbol{p}) + \boldsymbol{n}, \qquad (3)$$

where $\boldsymbol{F} = [\boldsymbol{f}_1, \ldots, \boldsymbol{f}_T] \in \mathbb{C}^{M\times T}$ with $\boldsymbol{f}_t = \boldsymbol{\Omega}_t \boldsymbol{a}(\boldsymbol{p}_{\mathrm{BS}}) \in \mathbb{C}^{M\times 1}$, and $\boldsymbol{\Omega}_t$ taking its values in the set of valid[2] RIS phase profiles:

$$|[\boldsymbol{f}_t]_m| = 1, \forall t, m. \qquad (4)$$

III. LOCALIZATION-OPTIMAL RIS PROFILE DESIGN

In this section, we show how RIS profiles can be optimized to minimize the PEB in a specific position. In Remark 1, we address how the resulting chicken-and-egg problem can be resolved (as the goal of designing the RIS profiles is to localize the user, while the design itself requires knowledge of the user's position).

A. FIM and PEB

We first define the vector of position and channel parameters in the 3D spherical coordinates system, as $\boldsymbol{\zeta}_{\mathrm{sph}} = [\rho, \theta, \phi, \beta_r, \beta_i]^{\top} \in \mathbb{R}^{5\times 1}$, and compute the FIM accordingly [16, Chapter 3.7]

$$\boldsymbol{J}_{\mathrm{sph}}(\boldsymbol{\zeta}_{\mathrm{sph}}) = \frac{2E_s}{N_0}\mathrm{Re}\left\{\left(\frac{\partial \boldsymbol{\mu}}{\partial \boldsymbol{\zeta}_{\mathrm{sph}}}\right)^{\mathsf{H}}\frac{\partial \boldsymbol{\mu}}{\partial \boldsymbol{\zeta}_{\mathrm{sph}}}\right\} \in \mathbb{R}^{5\times 5}, \qquad (5)$$

---

[1]Without loss of generality, we assume a constant pilot $x_t = \sqrt{E_s}$ is transmitted.

[2]So-called valid profiles correspond to practically feasible complex values according to real RIS hardware limitations (e.g., unit-modulus values with quantized phases).

where $\boldsymbol{\mu} = \beta \boldsymbol{F}^\top \boldsymbol{a}(\boldsymbol{p})$ denotes the noiseless part of the observation. To obtain the closed-form expressions of the FIM terms, we differentiate $\boldsymbol{\mu}$ with respect to the corresponding parameters

$$\left[\frac{\partial \boldsymbol{\mu}}{\partial \rho}, \frac{\partial \boldsymbol{\mu}}{\partial \theta}, \frac{\partial \boldsymbol{\mu}}{\partial \phi}\right] = \beta \boldsymbol{F}^\top \left[\dot{\boldsymbol{a}}_\rho(\boldsymbol{p}), \dot{\boldsymbol{a}}_\theta(\boldsymbol{p}), \dot{\boldsymbol{a}}_\phi(\boldsymbol{p})\right] \quad (6)$$

$$\left[\frac{\partial \boldsymbol{\mu}}{\partial \beta_r}, \frac{\partial \boldsymbol{\mu}}{\partial \beta_i}\right] = \boldsymbol{F}^\top \boldsymbol{a}(\boldsymbol{p})[1, \jmath], \quad (7)$$

where $\dot{\boldsymbol{a}}_x(\boldsymbol{p}) = \partial \boldsymbol{a}(\boldsymbol{p})/\partial x \in \mathbb{C}^{M \times 1}$. Then, introducing $\boldsymbol{\zeta}_{\text{car}} = [\boldsymbol{p}^\top, \beta_r, \beta_i]^\top \in \mathbb{R}^{5 \times 1}$ as the set of position and channel parameters in Cartesian coordinates system, we use the Jacobian $\boldsymbol{C} = \partial \boldsymbol{\zeta}_{\text{sph}}/\partial \boldsymbol{\zeta}_{\text{car}}$ to transform the previous FIM into

$$\boldsymbol{J}_{\text{car}}(\boldsymbol{\zeta}_{\text{car}}) = \boldsymbol{C}^\top \boldsymbol{J}_{\text{sph}}(\boldsymbol{\zeta}_{\text{sph}}) \boldsymbol{C}. \quad (8)$$

Finally, we characterize the positioning performance by means of the PEB, which is a lower bound on the accuracy of any unbiased location estimator, and is computed as [17, Chapter 2.4.2]

$$\text{PEB}(\boldsymbol{F}; \boldsymbol{\zeta}_{\text{car}}) = \sqrt{\text{tr}\left([\boldsymbol{J}_{\text{car}}^{-1}(\boldsymbol{\zeta}_{\text{car}})]_{(1:3, 1:3)}\right)} \quad (9)$$

$$\leq \sqrt{\mathbb{E}\{\|\boldsymbol{p} - \hat{\boldsymbol{p}}\|^2\}}, \quad (10)$$

where we have made the dependence of the precoding matrix $\boldsymbol{F}$ explicit.

B. PEB Minimization

Assuming prior knowledge of UE's position, we formulate the PEB optimization problem under a total power constraint, as follows

$$\min_{\boldsymbol{F}} \quad \text{PEB}(\boldsymbol{F}; \boldsymbol{\zeta}_{\text{car}}) \quad (11a)$$

$$\text{s.t.} \quad \text{tr}(\boldsymbol{F}\boldsymbol{F}^\mathsf{H}) = MT. \quad (11b)$$

We then suggest relaxing the above program: first, by using the change of variable $\boldsymbol{X} = \boldsymbol{F}\boldsymbol{F}^\mathsf{H}$ and then, by removing the constraint $\text{rank}(\boldsymbol{X}) = T$ [18, Chapter 7.5.2] [19], yielding

$$\min_{\boldsymbol{X}, \boldsymbol{u}} \quad \mathbf{1}^\top \boldsymbol{u} \quad (12a)$$

$$\text{s.t.} \quad \begin{bmatrix} \boldsymbol{J}_{\text{car}} & \boldsymbol{e}_k \\ \boldsymbol{e}_k^\top & u_k \end{bmatrix} \geq 0, k = 1, 2, 3, \quad (12b)$$

$$\text{tr}(\boldsymbol{X}) = MT, \quad (12c)$$

$$\boldsymbol{X} \geq 0, \quad (12d)$$

where $\boldsymbol{u} = [u_1, u_2, u_3]^\top$ is an auxiliary variable and $\boldsymbol{e}_k$ is the k-th column of the identity matrix. This optimization problem is a convex semidefinite program (SDP) since the FIM is a linear function of $\boldsymbol{X}$, as we can see from (5) to (8), and the constraints are either linear matrix inequalitys (LMIs) or linear equalities. According to [20, Appendix C], the optimal precoder covariance matrix $\boldsymbol{X}^\star$ is of the form

$$\boldsymbol{X}^\star = \boldsymbol{U}\boldsymbol{\Lambda}\boldsymbol{U}^\mathsf{H} \quad (13)$$

where $\boldsymbol{\Lambda} \in \mathbb{C}^{4 \times 4}$ is a positive semidefinite (PSD) matrix, denoting by its diagonal entries the beam weights applied to (or equivalently, the relative powers allocated to) the columns of $\boldsymbol{U}$ while

$$\boldsymbol{U} \triangleq [\boldsymbol{a}^*(\boldsymbol{p}) \ \dot{\boldsymbol{a}}_\rho^*(\boldsymbol{p}) \ \dot{\boldsymbol{a}}_\theta^*(\boldsymbol{p}) \ \dot{\boldsymbol{a}}_\phi^*(\boldsymbol{p})], \quad (14)$$

which are RIS steering vector and the successive derivative beams with respect to the spherical coordinates system components as that involved in (5). Note that the space spanned by the columns of $\boldsymbol{U}$ can also be spanned by 4 orthonormalized vectors, by applying the Gramm-Schmidt algorithm to the columns of $\boldsymbol{U}$, so that $\boldsymbol{U}^\mathsf{H}\boldsymbol{U} = M\boldsymbol{I}_4$. For the remainder of this paper, we will use these orthonormalized vectors, since the error bounds are function of the latter [19]. This allows us to write the constraint $\text{tr}(\boldsymbol{X}) = MT$ as $\text{tr}(\boldsymbol{\Lambda}) = T$. Applying the above transformation (i.e., from $\boldsymbol{X} \in \mathbb{C}^{M \times M}$ to $\boldsymbol{\Lambda} \in \mathbb{C}^{4 \times 4}$), the computational complexity is then significantly reduced, and the new optimization problem can be simply stated as

$$\min_{\boldsymbol{\Lambda}, \boldsymbol{u}} \quad \mathbf{1}^\top \boldsymbol{u} \quad (15a)$$

$$\text{s.t.} \quad \begin{bmatrix} \boldsymbol{J}_{\text{car}} & \boldsymbol{e}_k \\ \boldsymbol{e}_k^\top & u_k \end{bmatrix} \geq 0, k = 1, 2, 3, \quad (15b)$$

$$\text{tr}(\boldsymbol{\Lambda}) = T, \quad (15c)$$

$$\boldsymbol{\Lambda} \geq 0. \quad (15d)$$

Finally, the problem can be further relaxed by restricting $\boldsymbol{\Lambda}$ to be diagonal, i.e., $\boldsymbol{\Lambda} = \text{diag}(\boldsymbol{\lambda})$, in which case the entries in $\boldsymbol{\lambda}$ can be interpreted as power allocations or time units assigned to each column of $\boldsymbol{U}$. To solve the optimization problem (15), we used CVX [21].

Remark 1 (Assumption of prior knowledge): In a real system, perfect a priori knowledge of the UE location is not available, but can be reasonably approximated by the latest UE's estimated location (typically, while tracking the UE in the steady-state regime). In other words, we make use of this prior information to optimize the operating conditions for the next UE location estimate, given that the UE would be quasi-static in the meantime. Note that the presumed location uncertainty associated to this prior (if only made available by an estimator, e.g., as an error covariance or an uncertainty ellipse) can be taken into account in our optimization problem (11a), by minimizing the worst-case PEB in a region around the estimated UE location (i.e., in a set of points rather than in a single point), like in [22]. Furthermore, given a BS–RIS deployment, the optimization routine can be run offline and tabulated as a function of possible UE locations, so that the RIS profile can be reconfigured during the online phase at no extra computational cost, based on this location estimate.

C. Practical RIS Phase Profiles and Time Sharing

When solving the optimization problem above, multiple approaches can be taken to generate RIS phase profiles that satisfy the constraint (4). We limit our discussion to the case where $\boldsymbol{\Lambda} = \text{diag}(\boldsymbol{\lambda})$.

- *Optimize, then constrain:* from the optimal value $\boldsymbol{X}^\star = \boldsymbol{U}\boldsymbol{\Lambda}_{\text{opt}}\boldsymbol{U}^\mathsf{H}$ of (15), we transform the orthonormal beams in $\boldsymbol{U}$ into their unit-modulus versions (using gradient projections as in [23, Algorithm 1])
- *Constrain, then optimize:* in this approach, we first project the columns of $\boldsymbol{U}$ to satisfy the constraint (4) using the

parameter	value	parameter	value
f_c	28 GHz	wavelength	≈ 1.07 cm
W	120 kHz	UE loc. $\boldsymbol{p}$	$[1, 1...15, 1]$ m
N_0	-174 dBm/Hz	BS loc. $\boldsymbol{p}_{\text{BS}}$	$[5, 5, 0]$ m
noise figure n_f	8 dB	RIS loc. $\boldsymbol{p}_{\text{RIS}}$	$[0, 0, 0]$ m
P_{tx}	20 dBm	RIS size	$M = 32 \times 32$ elements
E_{tot}	$(P_{\text{tx}}/W)MT$	transmissions	$T = 40$

TABLE I: General simulation parameters.

same method from [23, Algorithm 1], and then solve (15) with the corresponding set of non-orthonormal vectors.

In either case, once (15) is solved and the set of precoders that satisfy (4) are determined, we aim to find time allocations T_i, $i \in \{1, 2, 3, 4\}$ subject to $\sum_{i=1}^{4} T_i = T$ and $T_i \in \mathbb{N}$, with $T_i \approx \lambda_i \in \mathbb{R}_+$. This problem can be solved by rounding λ_i to the nearest integer. Moreover, a more general allocation for arbitrary T can be found by solving (15) with $\text{tr}(\boldsymbol{\Lambda}) = 1$, in which case, the values $\lambda_i \in [0, 1]$ refer to the relative frequencies of the different RIS phase profiles. We can then set $T_i \approx \lambda_i T$, rounded to the nearest integer. With smaller T, the temporal quantization errors will become more pronounced, leading to PEB performance degradation. In particular, when $\lambda_i \ll 1$, the corresponding beam may never be selected, in which case the PEB will be infinite (since all 4 columns of $\boldsymbol{U}$ must be used). To address this, we force each column to be used at least once as a RIS phase configuration.

IV. SIMULATION RESULTS

A. Simulation Parameters

To assess the performance of the proposed design, several simulations have been performed in a canonical scenario, considering an indoor mmWave setting, using the parameters in Table I.

Remark 2 (Practical estimators): While our analysis is limited to performance bounds, it is expected that practical algorithms can achieve these bounds, when operating in a high SNR regime. Low-complexity NF localization methods were for instance discussed in [6], [24]. We also note that the proposed RIS phase profile designs involve only limited signaling or control overhead, since only the current user location needs to be provided to the RIS controller.

B. Performance Analysis

1) Visualization of Beams: In Fig. 3 (a)–(c), we first show the four orthonormalized beams applied at the reflective RIS (i.e., the directional beam and its derivatives), as a function of the 3 spherical coordinates. To elaborate, the figure displays a so-called *Gain*, which corresponds to the expression $|\boldsymbol{u}^\top \boldsymbol{a}(\tilde{\boldsymbol{p}})|^2$, where $\boldsymbol{u}$ represents a column in $\boldsymbol{U}$ and $\tilde{\boldsymbol{p}}$ is an arbitrary test location. The columns of $\boldsymbol{U}$ are generated according to (14) with $\boldsymbol{p} = [1, 2, 1]^\top$. For visualization purposes, we show cuts of possible positions $\tilde{\boldsymbol{p}}$ along the three polar coordinates, fixing the other two coordinates to the corresponding values of $\boldsymbol{p} = [1, 2, 1]^\top$. As expected and similar to [22], it is noticed that the beam derivatives get their null values at the actual UE range/direction and that each beam null is visible in the three dimensions. These nulls lead to significant variation around the position to be estimated, thereby improving the

(a) Beam responses vs. θ with θ_{UE} denoting the UE azimuth angle.

(b) Beam responses vs. ϕ with ϕ_{UE} denoting the UE elevation angle.

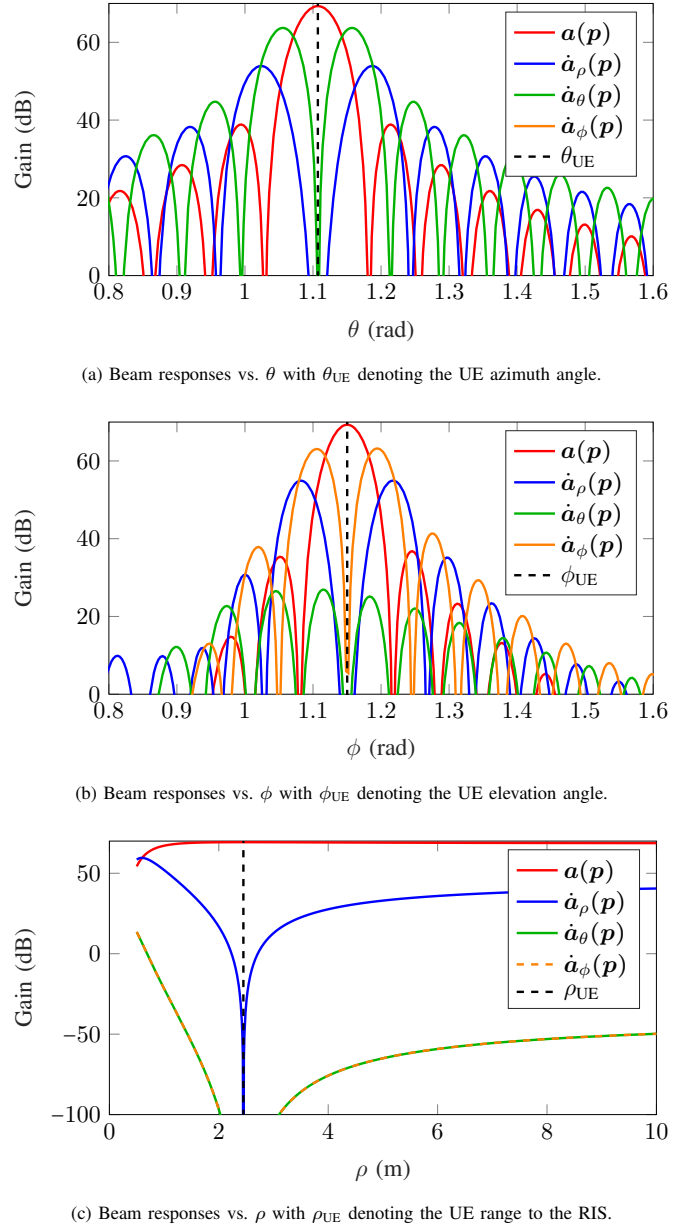(c) Beam responses vs. ρ with ρ_{UE} denoting the UE range to the RIS.

Fig. 3: Orthonormalized beams applied at the reflective RIS as a function of the three polar coordinates (incl. the directional beam and its derivatives).

positioning accuracy. In particular, the variation with respect to $x \in \{\theta, \phi, \rho\}$ is most pronounced for the beam $\dot{\boldsymbol{a}}_x(\boldsymbol{p})$.

2) Comparison of Design Strategies: In Fig. 4, as a function of the RIS-UE distance, we then compare the PEB achievable with the optimal design (i.e., under unconstrained $\boldsymbol{\Lambda}$) with that obtained with purely random RIS phase profiles [7] and directional RIS beams [6]. In the latter approach, directional RIS beams are generated uniformly distributed into a sphere centered around the actual UE position, while assuming different levels of uncertainty (i.e., different values for the sphere radius r). The total energy was fixed to make the comparison fair among the different schemes. We first observe that the optimal design systemically outperforms the two other designs, whatever the distance. As for random phase profiles more
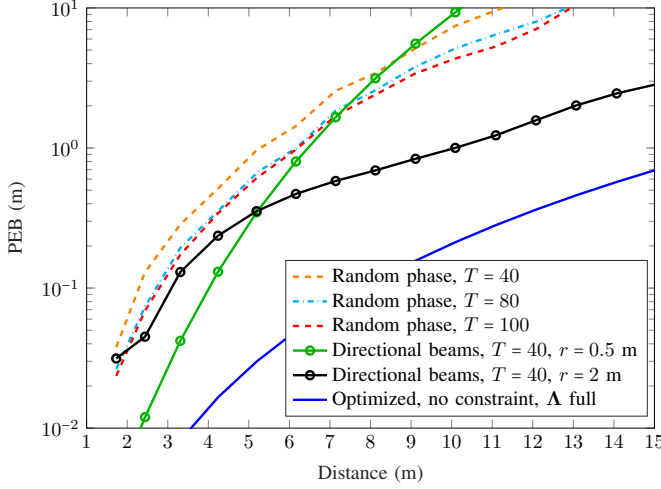
Fig. 4: PEB comparison as a function of the RIS-UE distance, for optimized RIS phase profiles (with optimal $\mathbf{\Lambda}$), random RIS phase profiles and directional RIS beams (for different numbers of transmissions T and uncertainty levels r).

specifically, beyond a certain number of transmissions (say, around 80 in the shown example), no further spatial diversity can be brought into the problem by the new profiles (i.e., most of the space has already been covered by previous profiles) so that performance asymptotically reaches a limit. With directional beams, the effect of prior UE location uncertainty is rather remarkable. Smaller uncertainty (i.e., $r = 0.5$ m) indeed provides much better results at short distances (even close to the optimal design) but conversely leads to poor angular diversity and hence becomes counterproductive at long distances, just as if a unique beam was always selected to point in the same direction over all the transmissions.

3) Feasible RIS Profiles: Fig. 5 provides a benchmark of the achievable PEB as a function of the distance with different variants of the problem solver, as described in Section III-C, assuming both full and diagonal $\mathbf{\Lambda}$, considering both *constrain, then optimize*, and *optimize, then constrain* approaches. Forcing $\mathbf{\Lambda}$ to be diagonal in the optimization has almost no effect on the results in comparison with unconstrained $\mathbf{\Lambda}$. This is likely due to the fact that the initial beam vectors in $\boldsymbol{U}$ are orthogonal and hence, $\mathbf{\Lambda}$ shall be structurally quasi-diagonal accordingly. Constraining before optimization turns out to be superior over constraining after optimization. Hence, we will consider the former approach from now on. Fig. 6 shows the corresponding output of the optimizer in terms of λ_i values, as a function of the RIS–UE distance. We notice that there is a strong dependence on the derivative beam with respect to the range. Moreover, as the UE moves away from the RIS, we see less reliance on the angular derivative beams whose weights become nearly negligible, but almost a uniform dependence on directional. Finally. in Fig. 7, we show the PEB achievable with our optimized design as a function of the RIS-UE distance, for both optimal $\mathbf{\Lambda}$ and its practical implementation through time sharing (depicted as "Time division" here, see Section III-C) for distinct T values, where the i-th beam is such that $\boldsymbol{f}_i$ is forced to lie onto the unit
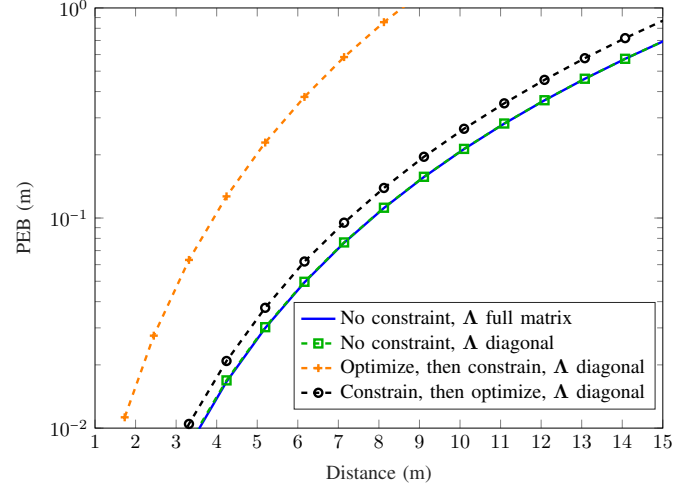

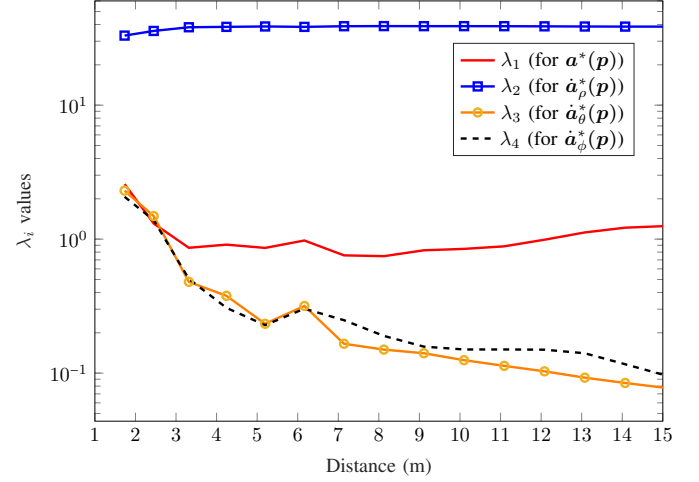Fig. 5: Achievable PEB as a function of the distance for different variants of the problem solver.

Fig. 6: Diagonal terms of $\mathbf{\Lambda}_{\text{opt}}$ accounting for the different beam weights, as a function of the RIS-UE distance.

circle and used over T_i transmissions out of T. As expected, lower values of T lead to worse performance, as the temporal quantization effect is more pronounced. Inversely, as the value of T increases the performance approaches, asymptotically, that of the optimized $\mathbf{\Lambda}$.

C. Complexity

Despite the possibility to generate and tabulate offline PEB-optimal RIS profiles as a function of the UE location so as to reduce the online computational cost (See Remark 1), we now assess how the optimization problem scales with RIS size M. Calculating both directional and derivative beams has a complexity of $\mathcal{O}(M)$. Projecting the beams to the unit-modulus space has also a complexity of $\mathcal{O}(M)$. More precisely, this step has a complexity $\mathcal{O}(NM/\epsilon)$, where N is the number of 3D points chosen in [23, Algorithm 1], and ϵ is the accuracy limit for the algorithm convergence. Calculating the optimal $\mathbf{\Lambda}$ in our case is independent of M. So overall, the complexity is of order $\mathcal{O}(M)$, which is the same as that of directional codebooks. Beyond, for practical beamforming
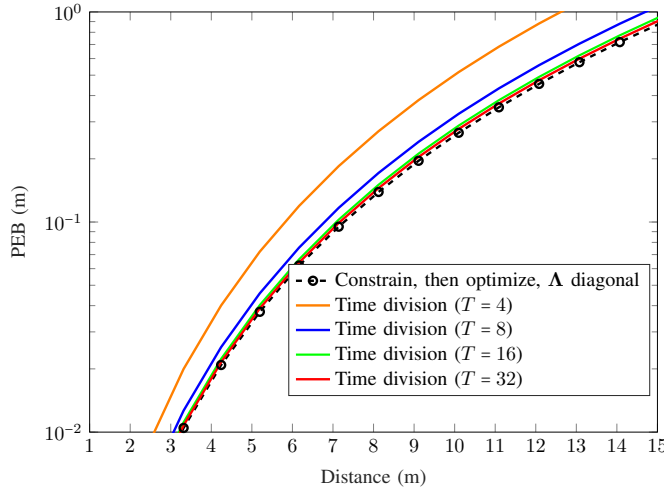
Fig. 7: Achievable PEB as a function of the RIS-UE distance with both optimal diagonal $\mathbf{\Lambda}$ and its practical implementation through time sharing depending on T (i.e., so-called "Time division", allocating T_i over T transmissions for the i-th feasible beam separately, with related $\boldsymbol{f}_i$ forced onto the unit circle).

anyway, one does not need to calculate explicitly $\boldsymbol{X}$ but just to repeat beams based on optimized terms in $\mathbf{\Lambda}$.

V. CONCLUSIONS

In this paper, we have described a reflective RIS phase profile design minimizing the PEB of NLoS localization over downlink SISO narrowband transmissions, while considering a generic near-field formalism for the RIS response. On this occasion, we have shown that the theoretical optimal solution would involve the combination of four weighted beams at the RIS, whose practical performance in terms of achievable PEB has been evaluated while considering more realistic unit-modulus beams. Finally, for the sake of implementability, we have also introduced a time sharing scheme, assuming the application of each feasible beam sequentially, with very limited performance degradation whenever the overall number of transmissions is sufficiently large. Future work will consider the evaluation of practical point estimators and tracking algorithms that use the proposed RIS phase profiles, the approximation of the required sequential beams under real reflective RIS hardware characterization [25], as well as the extension to multi-user and multi-RIS contexts.

ACKNOWLEDGMENT

REFERENCES

[1] E. C. Strinati, G. C. Alexandropoulos, H. Wymeersch, B. Denis, V. Sciancalepore, R. D'Errico, A. Clemente, D.-T. Phan-Huy, E. De Carvalho, and P. Popovski, "Reconfigurable, Intelligent, and Sustainable Wireless Environments for 6G Smart Connectivity," *IEEE Communications Magazine*, vol. 59, no. 10, pp. 99–105, 2021.

[2] H. Wymeersch, J. He, B. Denis, A. Clemente, and M. Juntti, "Radio localization and mapping with reconfigurable intelligent surfaces: Challenges, opportunities, and research directions," *IEEE Vehicular Technology Magazine*, vol. 15, no. 4, pp. 52–61, 2020.

[3] S. Hu, F. Rusek, and O. Edfors, "Beyond massive MIMO: The potential of positioning with large intelligent surfaces," *IEEE Transactions on Signal Processing*, vol. 66, no. 7, pp. 1761–1774, 2018.

[4] J. V. Alegría and F. Rusek, "Cramér-Rao lower bounds for positioning with large intelligent surfaces using quantized amplitude and phase," in *2019 53rd Asilomar Conference on Signals, Systems, and Computers*, pp. 10–14, 2019.

[5] F. Guidi and D. Dardari, "Radio positioning with EM processing of the spherical wavefront," *IEEE Transactions on Wireless Communications*, vol. 20, no. 6, pp. 3571–3586, 2021.

[6] Z. Abu-Shaban, K. Keykhosravi, M. F. Keskin, G. C. Alexandropoulos, G. Seco-Granados, and H. Wymeersch, "Near-field localization with a reconfigurable intelligent surface acting as lens," in *IEEE International Conference on Communications (ICC)*, 2021.

[7] H. Wymeersch and B. Denis, "Beyond 5G Wireless Localization with Reconfigurable Intelligent Surfaces," in *IEEE International Conference on Communications (ICC)*, June 2020.

[8] A. Elzanaty, A. Guerra, F. Guidi, and M.-S. Alouini, "Reconfigurable intelligent surfaces for localization: Position and orientation error bounds," *IEEE Transactions on Signal Processing*, vol. 69, pp. 5386–5402, 2021.

[9] J. He, H. Wymeersch, L. Kong, O. Silvén, and M. Juntti, "Large intelligent surface for positioning in millimeter wave mimo systems," in *IEEE Vehicular Technology Conference (VTC)*, 2020.

[10] H. Zhang, H. Zhang, B. Di, K. Bian, Z. Han, and L. Song, "Towards ubiquitous positioning by leveraging reconfigurable intelligent surface," *IEEE Communications Letters*, vol. 25, no. 1, pp. 284–288, 2021.

[11] K. Keykhosravi, M. F. Keskin, G. Seco-Granados, and H. Wymeersch, "SISO RIS-enabled joint 3D downlink localization and synchronization," in *IEEE International Conference on Communications (ICC)*, 2021.

[12] M. Rahal, B. Denis, K. Keykhosravi, B. Uguen, and H. Wymeersch, "RIS-enabled localization continuity under near-field conditions," in *IEEE International Workshop on Signal Processing Advances in Wireless Communications (SPAWC)*, pp. 436–440, 2021.

[13] Y. Liu, E. Liu, R. Wang, and Y. Geng, "Reconfigurable intelligent surface aided wireless localization," in *IEEE International Conference on Communications (ICC)*, 2021.

[14] A. Abrardo, D. Dardari, and M. Di Renzo, "Intelligent reflecting surfaces: Sum-rate optimization based on statistical position information," *IEEE Transactions on Communications*, vol. 69, no. 10, pp. 7121–7136, 2021.

[15] X. Hu, C. Zhong, Y. Zhang, X. Chen, and Z. Zhang, "Location information aided multiple intelligent reflecting surface systems," *IEEE Transactions on Communications*, vol. 68, no. 12, pp. 7948–7962, 2020.

[16] S. Kay, *Fundamentals of Statistical Signal Processing: Practical algorithm development*. Fundamentals of Statistical Signal Processing, Prentice-Hall PTR, 2013.

[17] H. Van Trees, *Detection, Estimation, and Modulation Theory, Part I: Detection, Estimation, and Linear Modulation Theory*. No. pt. 1, Wiley & Sons, Ltd, 2004.

[18] S. Boyd and L. Vandenberghe, *Convex optimization*. Cambridge university press, 2004.

[19] N. Garcia, H. Wymeersch, and D. T. M. Slock, "Optimal precoders for tracking the aod and aoa of a mmwave path," *IEEE Transactions on Signal Processing*, vol. 66, no. 21, pp. 5718–5729, 2018.

[20] J. Li, L. Xu, P. Stoica, K. W. Forsythe, and D. W. Bliss, "Range compression and waveform optimization for MIMO radar: A Cramér–Rao bound based study," *IEEE Transactions on Signal Processing*, vol. 56, no. 1, pp. 218–232, 2008.

[21] M. Grant and S. Boyd, "CVX: Matlab software for disciplined convex programming, version 2.1." http://cvxr.com/cvx, Mar. 2014.

[22] M. F. Keskin, F. Jiang, F. Munier, G. Seco-Granados, and H. Wymeersch, "Optimal Spatial Signal Design for mmWave Positioning under Imperfect Synchronization," *IEEE Transactions on Vehicular Technology*, 2022. arXiv: 2105.07664.

[23] J. Tranter, N. D. Sidiropoulos, X. Fu, and A. Swami, "Fast unit-modulus least squares with applications in beamforming," *IEEE Transactions on Signal Processing*, vol. 65, no. 11, pp. 2875–2887, 2017.

[24] O. Rinchi, A. Elzanaty, and M.-S. Alouini, "Compressive near-field localization for multipath RIS-aided environments," *IEEE Communications Letters*, 2022.

[25] M. Rahal, B. Denis, K. Keykhosravi, F. Keskin, B. Uguen, G. C. Alexandropoulos, and H. Wymeersch, "Arbitrary beam pattern approximation via riss with measured element responses," arXiv: 2203.07225.